

# Mem-fractive Properties of Mushrooms

Alexander E. Beasley<sup>\*1,\*</sup>, Mohammed-Salah Abdelouahab<sup>3</sup>, René Lozi<sup>2</sup>, Anna L. Powell<sup>1</sup>,  
and Andrew Adamatzky<sup>1</sup>

<sup>1</sup>*Unconventional Computing Laboratory, UWE, Bristol, UK*

<sup>2</sup>*Université Côte d'Azur, CNRS, LJAD, Nice, France*

<sup>3</sup>*Laboratory of Mathematics and their interactions, University Centre Abdelhafid Boussouf,  
Mila 43000, Algeria*

## Abstract

Memristors close the loop for I-V characteristics of the traditional, passive, semi-conductor devices. Originally proposed in 1971, the hunt for the memristor has been going ever since. The key feature of a memristor is that its current resistance is a function of its previous resistance and the current passed through it. As such, the behaviour of the device is influenced by changing the way in which potential is applied across it. Ultimately, information can be encoded on memristors. Biological substrates have already been shown to exhibit some memristive properties. By extension, the mem-capacitor and mem-inductor have been proposed. Such devices change either their capacitive or inductive properties a function of the previous voltage, similar to memristors. A device that exhibits combinations of memristors, mem-capacitors and mem-inductors is termed a mem-fractive device. However, many passive memory devices are yet to be found. Here we show that the fruit bodies of grey oyster fungi *Pleurotus ostreatus* exhibit encouraging behaviour in the field of organic memory devices. This paper presents the I-V characteristics of the mushrooms. By examination of the conducted current for a given voltage applied as a function of the previous voltage, it is shown that the mushroom exhibits the properties of a mem-fractor. Our results demonstrate that nature continues to provide specimens that hold these unique and valuable electrical characteristics and which have the potential to advance the field of hybrid electronic systems.

Keywords: memristor, fungi, memfractance

## 1 Introduction

Originally proposed by Chua in 1971 [10], the memristor poses a fourth basic circuit element, whose characteristics differ from that of R, L and C elements. Memristance has been seen in nano-scale devices where electronic and ionic transport are coupled under an external bias voltage [35]. Strukov *et al.* posit that the hysteric I-V characteristics observed in thin-film, two-terminal devices can be understood as memristive. However, this is observed behaviour of devices that already have other, large signal behaviours.

Finding a true memristor is by no means an easy task. Nevertheless, a number of studies have turned to nature to provide the answer, with varying success. Memristive properties of organic polymers were discovered well before the ‘official’ discovery of the memristor was announced in [35]. The first examples of memristors could go back to the singing arc, invented by Duddell in 1900, and originally used in wireless telegraphy before the invention of the triode [18]. Memristive properties of organic polymers have been studied since 2005 [13] in experiments with hybrid electronic devices based on polyaniline-polyethylenoxide junction [13]. Memristive properties of living creatures and their organs and fluids have been demonstrated in skin [29], blood [24], plants [37] (including fruits [36]), slime mould [15], tubulin microtubules [12, 9].

---

\*Corresponding author: Alexander Beasley, alex.beasley@uwe.ac.uk

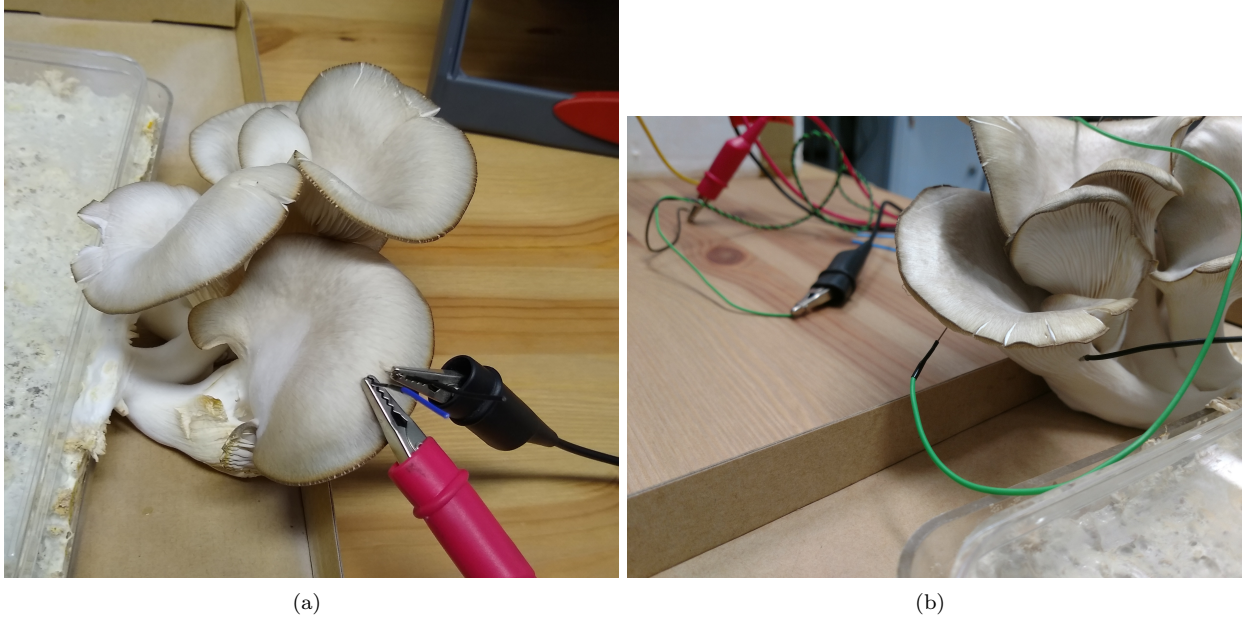


Figure 1: Positions of electrodes in fruit bodies. (a) Electrodes inserted 10 mm apart in the fruit body cap. (b) One electrode is inserted in the cap with the other in the stem.

This paper presents a study of the I-V characteristics of the fruit bodies of the grey oyster fungi *Pleurotus ostreatus*. Why fungi? Previously we recorded extracellular electrical potential of oyster’s fruit bodies, basidiocarps [2] and found that the fungi generate action potential like impulses of electrical potential. The impulses can propagate as isolated events, or in trains of similar impulses. Further, we demonstrated, albeit in numerical modelling, that fungi can be used as computing devices, where information is represented by spikes of electrical activity, a computation is implemented in a mycelium network and an interface is realised via fruit bodies [3]. A computation with fungi might not be useful *per se*, because the speed of spike propagation is substantially lower than the clock speed in conventional computers. However, the fungal computation becomes practically feasible when embedded in a slow developing spatial process, e.g. growing architecture structures. Thus, in [4] we discussed how to: produce adaptive building constructions by developing structural substrate using live fungal mycelium, functionalising the substrate with nanoparticles and polymers to make mycelium-based electronics, implementing sensorial fusion and decision making in the fungal electronics.

Why we are looking for mem-fractive properties of fungi? Mem-fractors [1] have combinations of properties exhibited by memristors, mem-capacitors and mem-inductors. A memristor is a material implication [7, 26] and can, therefore, can be used for constructing other logical circuits, statefull logic operations [7], logic operations in passive crossbar arrays of memristors [28], memory aided logic circuits [25], self-programmable logic circuits [6], and, indeed, memory devices [19]. If strands of fungal mycelium in a culture substrate and the fruit bodies show some mem-fractive properties then we can implement a large variety of memory and computing devices embedded directly into architectural building materials made from the fungal substrates [4].

The rest of this paper is organised as follows. Section 2 details the experimental set up used to examine the I-V characteristics of fruit bodies. Section 3 presents the results from the experimentation, with further discussion of voltage spiking provided in section 3.2. Mathematical modelling of the mem-fractive behaviour of the Grey Oyster mushrooms is given in section 4. A discussion of the results is given in section 5 and finally conclusions are given in section 3.

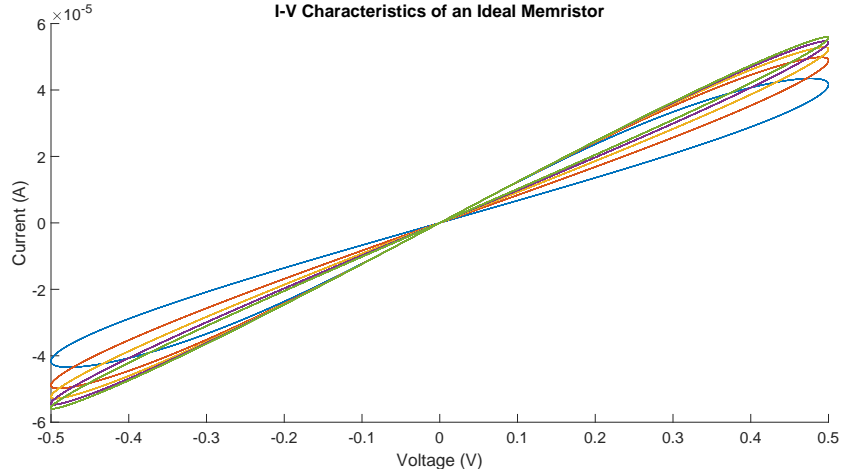


Figure 2: I-V Characteristics from a model of an ideal memristor [20].

## 2 Experimental Set Up

We used grey oyster fungi *Pleurotus ostreatus* (Ann Miller’s Speciality Mushrooms Ltd, UK) cultivated on wood shavings. The iridium-coated stainless steel sub-dermal needles with twisted cables (Spes Medica SRL, Italy) were inserted in fruit bodies (Fig. 1) of grey oyster fungi using two different arrangements: 10 mm apart in the cap of the fungi (cap-to-cap), Fig. 1(a), and translocation zones (cap-to-stem), Fig. 1(b). I-V sweeps were performed on the fungi samples with Keithley Source Measure Unit (SMU) 2450 (Keithley Instruments, USA) under the following conditions: [-500 mV to 500 mV, -1 V to 1 V] with the samples in ambient lab light (965 Lux). Varying the step size of the voltage sweep allowed testing the I-V characteristics of the subject at different frequencies. Electrodes were arranged in two different methods: both electrodes approximately 10 mm apart in the cap of the fruit body (Fig. 1(a)); and one electrode placed in the cap with the other electrode placed in the stem (Fig. 1(b)). The voltage ranges are limited so as not to cause the electrolysis of water. Each condition was repeated at least six times over the samples. Voltage sweeps were performed in both directions (cyclic voltammetry) and plots of the I-V characteristics were produced.

MATLAB was used to analyse the frequency and distribution of spiking behaviour observed in the I-V sweeps of the fruiting bodies under test (Sect. 3.2). All histogram plots are binned according to the voltage interval set for the Kiethley SMU.

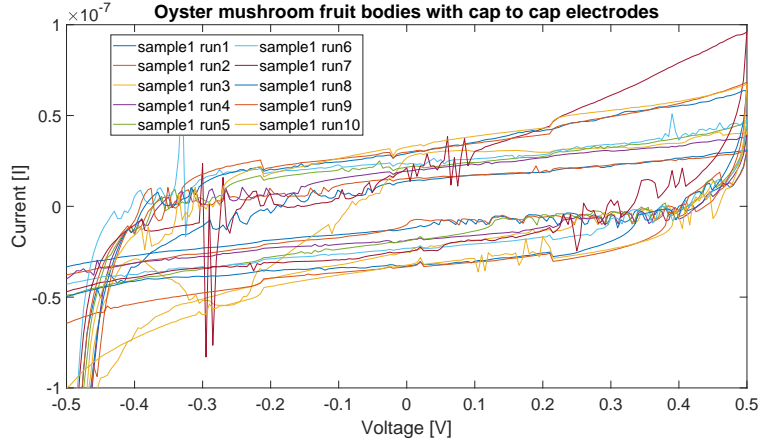
## 3 Results

### 3.1 I-V characterisation

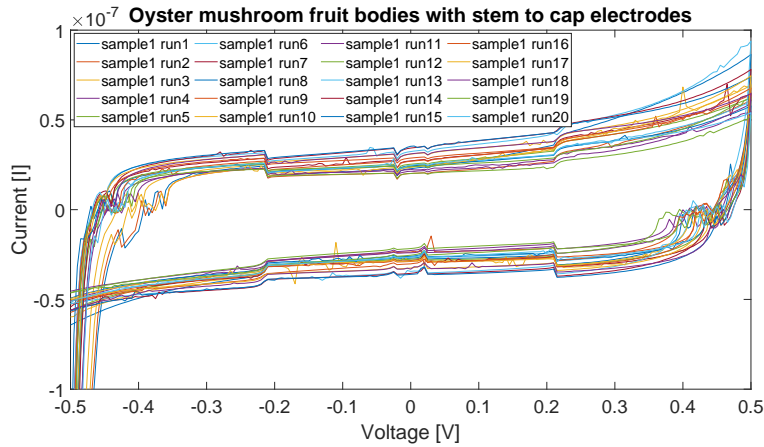
Fruit body samples are shown to exhibit memristive properties when subject to a voltage sweep. The ideal memristor model (Fig. 2) is shown to display ‘lobes’ on the I-V characterisation sweeps, indicating that the current resistance is a function of the previous resistance — hence a memristor has memory. For the purposes of analysis, graphs are referred to by their quadrants, starting with quadrant one as the top right and being number anti-clockwise.

The ideal memristor model has a crossing point at 0V, where theoretically no current flows. From Figs. 3 and 4, it can be seen that when 0 V is applied by the source meter, a reading of a nominally small voltage and current is performed. The living membrane is capable of generating potential across the electrodes, and hence a small current is observed. Mem-capacitors produce similar curves to that in Fig. 2, when plotting charge ( $q$ ) against voltage ( $v$ ) [38]. Additionally, mem-inductors produce similar plots for current ( $i$ ) against flux ( $\varphi$ ).

While the sample under test is subjected to a positive voltage (quadrant 1), it can be seen there is nominally a positive current flow. Higher voltages result in a larger current flow. For an increasing voltage



(a)



(b)

Figure 3: Raw data from cyclic voltammetry performed over  $-0.5$  V to  $0.5$  V. (a) Cap-to-cap electrode placement. (b) Stem-to-cap electrode placement.

sweep there is a larger current flow for the corresponding voltage during a negative sweep.

Similarly, in quadrant 3 where there is a negative potential across the electrodes, the increasing voltage sweep yields a current with smaller magnitude than the magnitude of the current on a negative voltage sweep.

Put simply, the fruit body has a resistance that is a function of the previous voltage conditions.

By applying averaging to the performed tests, a clear picture is produced that demonstrates for a given set of conditions, a typical response shape can be expected (Figs. 5 and 6). The stem-to-cap placement of the electrodes in the fruit body yields a tighter range for the response (figures 5(b) and 6(b)). This can be expected due to the arrangement of the transportation pathways, so-called translocation zone distinct from any vascular hyphae [33, 23], in the fruit body which run from the edge of the cap and down back through the stem to the root structure (mycelium). Cap-to-cap placement of the electrodes applies the potential across a number of the solutes translocation pathways and hence yields a wider range of results. However, for all results, it is observed that the positive phase of the cyclic voltammetry produces a different conducted current than the negative phase. The opening of the hysteresis curve around the zero, zero point suggests the fungus is not strictly a mem-ristor, instead it is also exhibiting mem-capacitor and mem-inductor effects. The build of charge in the device prevents the curve from closing completely to produce the classic mem-ristor pinching shape.

Reducing the step voltage step size (by ten fold) for the I-V characterisation is synonymous to reducing

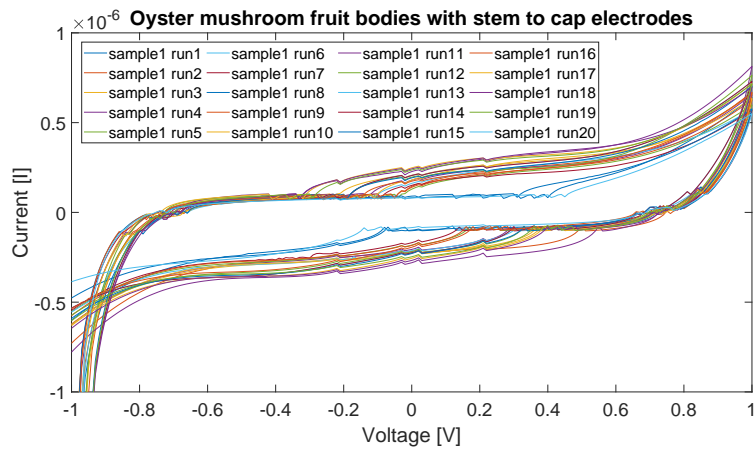
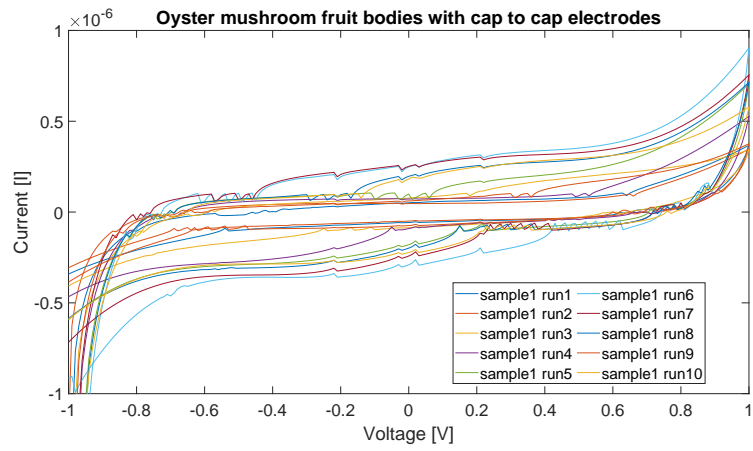
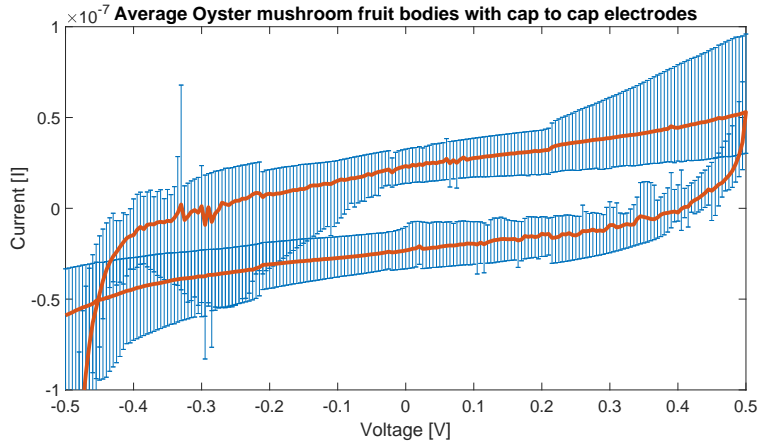
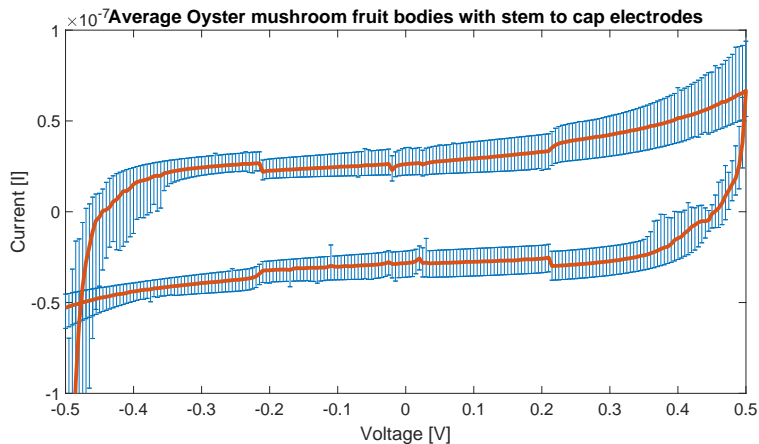


Figure 4: Raw data from cyclic voltammetry performed over -1 V to 1 V. (a) Cap-to-cap electrode placement. (b) Stem-to-cap electrode placement.



(a)



(b)

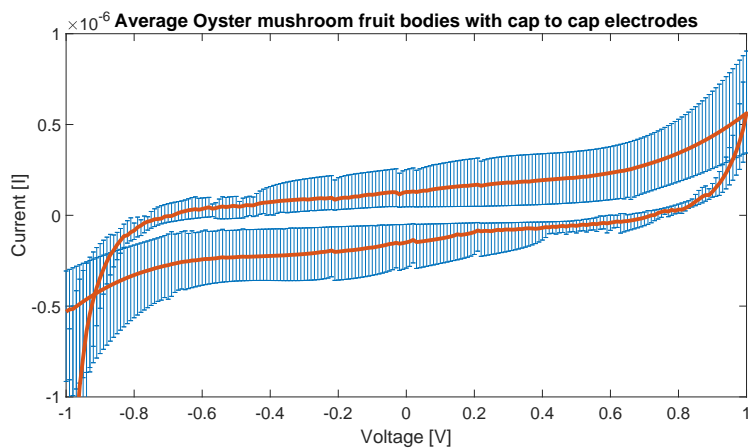
Figure 5: Average grey oyster fungi fruit bodies I-V characteristics for cyclic voltammetry of -0.5 V to 0.5 V. (a) Cap-to-cap electrode placement. (b) Stem-to-cap electrode placement.

the frequency of the voltage sweep. Decreasing the sweep frequency of the voltage causes the chances of “pinching” in the I-V sweep to increase, as seen in quadrant 1 of figure 7. This further reinforces the presence of some mem-capacitor behaviour. Since the charging frequency of the fungus has now been reduced there is a greater amount of time for capacitively stored energy to dissipate, thus producing a more ‘resistive’ plot with a pinch in the hysteresis.

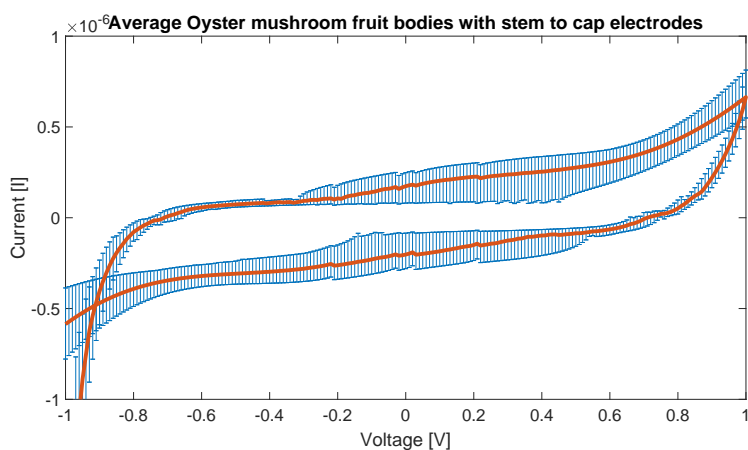
### 3.2 Spiking

It is observed from Figs. 3 to 4 that portions of the cyclic voltammetry result in oscillations in the conducted current, or spiking activity. Oscillations occur most prominently on the positive phase of the cyclic voltammetry as the applied voltage approaches 0V and similarly on the negative phase, again as the applied voltage approaches 0 V. Current oscillations are typically in the order of nano-amps and persist for a greater number of cycles when the electrodes are arranged as a pair on the fruit body cap (between five and ten cycles) compared to the stem-to-cap arrangement (fewer than five repeats).

Figure 8 demonstrates the spiking frequency of a single repeat of the cyclic voltammetry performed between -0.5 V and 0.5 V with the electrodes in a cap-to-cap arrangement. It is shown in the figure that



(a)



(b)

Figure 6: Average fruit bodies I-V characteristics for cyclic voltammetry of -1 V to 1 V. (a) Cap-to-cap electrode placement. (b) Stem-to-cap electrode placement.

the voltage interval between spikes in an oscillation period are less than 0.06 V. Figure 9 concatenates the data for all repeats of the cyclic voltammetry performed under four different conditions. It is clearly shown that in cap-to-cap arrangements the voltage interval between spikes is less than when the electrodes are in a translocation arrangement. Any spikes that occur when the voltage interval becomes large can be taken as not occurring during a period of oscillation in the sweep, instead they occur infrequently and randomly during the sweep.

Reducing the frequency of the voltage sweep (Fig. 7) also has the effect of removing the current oscillations.

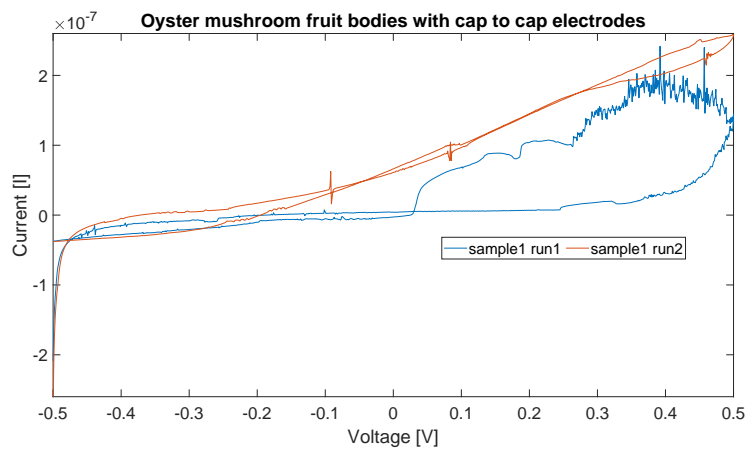


Figure 7: I-V Characteristics of fungi fruit bodies with the voltage step size set to 0.001 V.

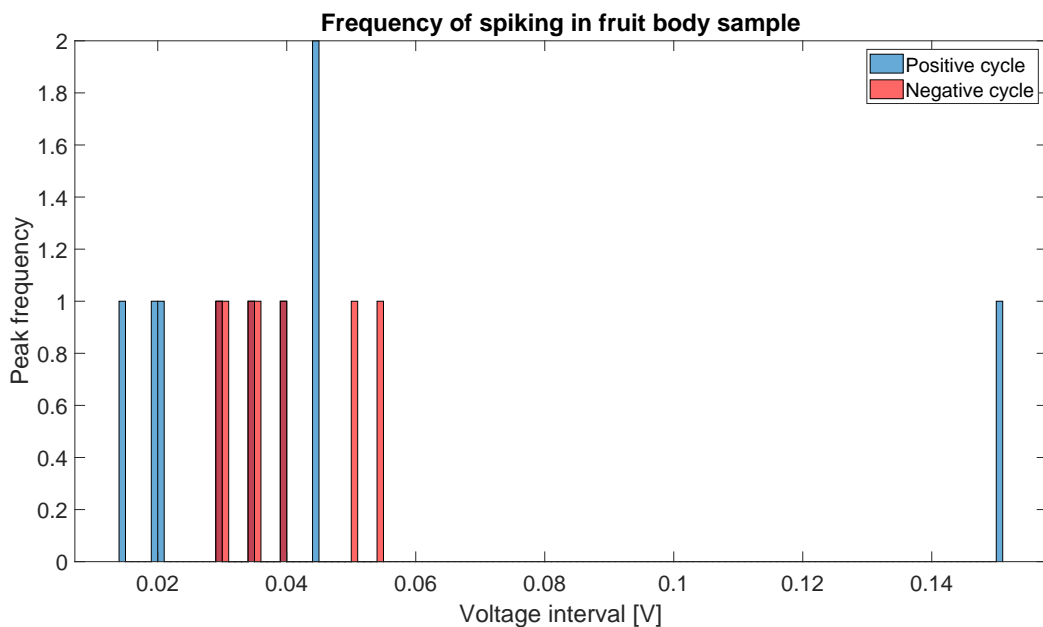


Figure 8: The voltage interval of spikes in the I-V characteristics of the fruit body for a single run.

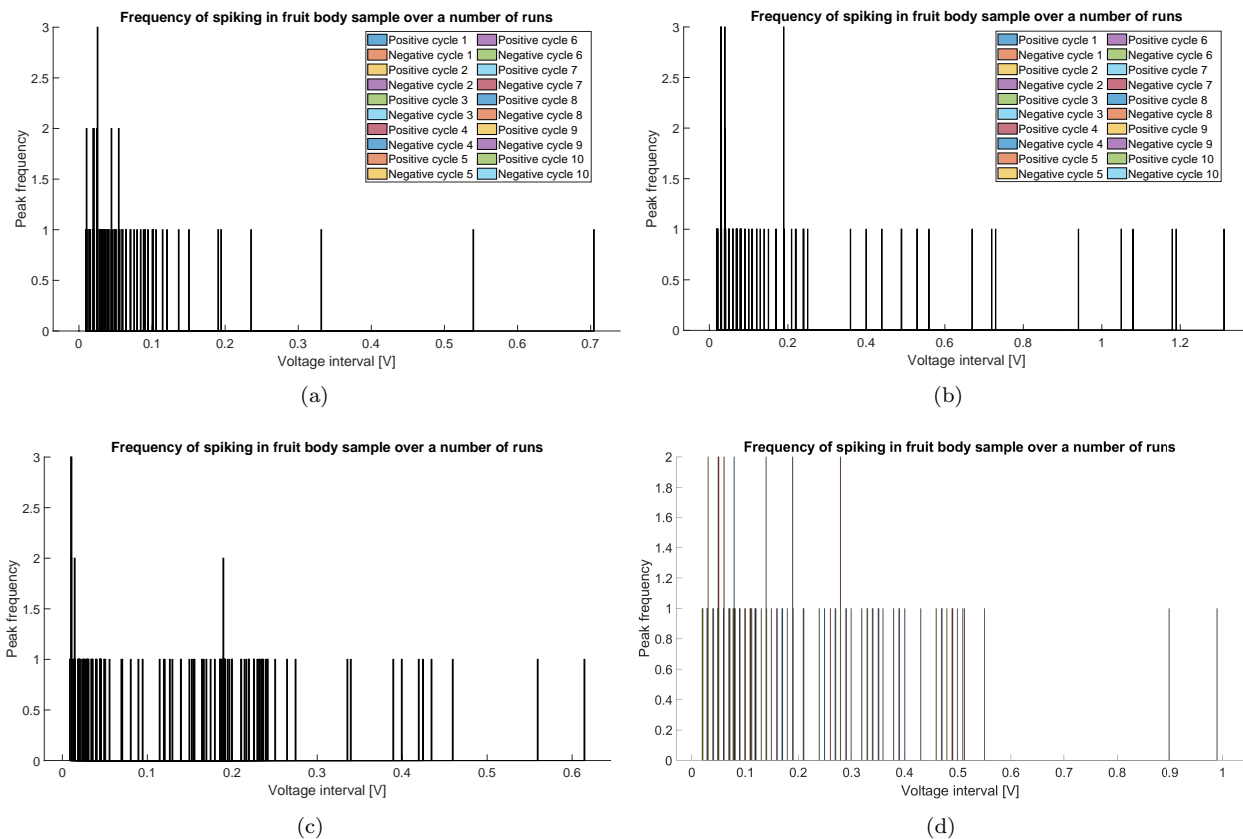


Figure 9: Concatenations of all spiking data from all data runs for four different test conditions. (a) voltammetry over -0.5 V to 0.5 V, cap-to-cap electrode arrangement. (b) voltammetry over -1 V to 1 V, cap-to-cap electrode arrangement. (c) voltammetry over -0.5 V to 0.5 V, stem-to-cap electrode arrangement. (d) voltammetry over -1 V to 1 V, stem-to-cap electrode arrangement. Legends omitted on (c) and (d) for clarity.

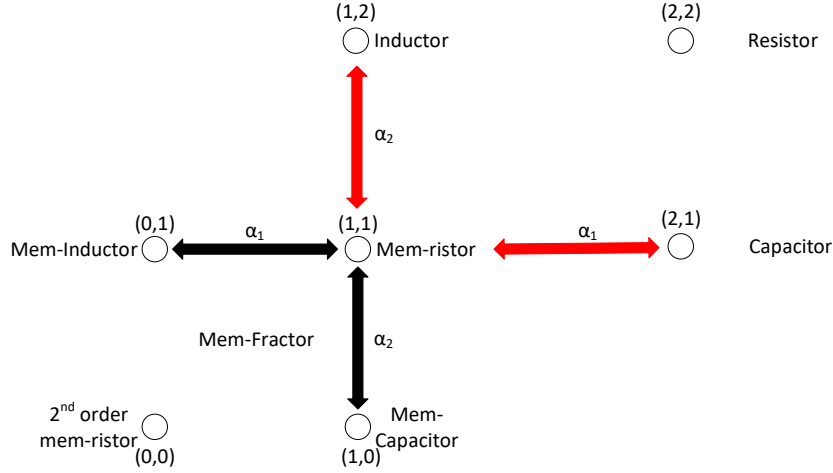


Figure 10: Non-binary solution space showing mem-fractive properties of a memory element

## 4 Mathematical Model of Mushroom Memfractance

Here we report the I-V characteristics of grey oyster fungi *Pleurotus ostreatus* fruit bodies. It is evident from the results that grey oyster fungi display memristive behaviour.

Although the fruit bodies typically do not demonstrate the “pinching” property of an ideal memristor [11], it can be clearly seen that the biological matter exhibits memory properties when the electrical potential across the substrate is swept. A positive sweep yields a higher magnitude current when the applied voltage is positive; and a smaller magnitude current when the applied voltage is negative.

Fractional Order Memory Elements (FOME) are proposed as a combination of Fractional Order Mem-Capacitors (FOMC) and Fractional Order Mem-Inductors (FOMI) [1]. The FOME (1) is based on the generalised Ohm’s law and parameterised as follows:  $\alpha_1, \alpha_2$  are arbitrary real numbers — it is proposed that  $0 \geq \alpha_1, \alpha_2 \leq 1$  models the solution space by [5],  $F_M^{\alpha_1, \alpha_2}$  is the memfractance,  $q(t)$  is the time dependent charge,  $\varphi(t)$  is the time dependent flux. Therefore, the memfractance ( $F_M^{\alpha_1, \alpha_2}$ ) is an interpolation between four points:  $MC$  — mem-capacitance,  $R_M$  — memristor,  $MI$  — mem-inductance, and  $R_{2M}$  — the second order memristor. Full derivations for the generalised FOME model are given by [1, 5]. The definition of memfractance can be straightforward generalised to any value of  $\alpha_1, \alpha_2$  (see [1, Fig. 27]).

$$D_t^{\alpha_1} \varphi(t) = F_M^{\alpha_1, \alpha_2}(t) D_t^{\alpha_2} q(t) \quad (1)$$

The appearance of characteristics from various memory elements in the fungal I-V curves supports the assertion that the fungal is a mem-fractor where  $\alpha_1$  and  $\alpha_2$  are both greater than 0 and less than 2.

There is no biological reason for memfractance of Ooyster fungi fruit bodies with stem to cap electrodes, be a usual closed formula. Therefore, one can get only a mathematical approximation of this function. In this section, we propose two alternatives to obtain the best approximation for memfractance in the case of average fruit bodies I-V characteristics for cyclic voltammetry of Fig. 6(b) (Fig. 11).

### 4.1 Approximation by polynomial on the whole interval of voltage

Raw data include the time, voltage and intensity of each reading. There are 171 readings for each run. The process of these data, in order to obtain a mathematical approximation of memfractance, in the first alternative, takes 4 steps as follows. First step: approximate  $v(t)$  by a twenty-four-degree polynomial (Fig. 12) whose coefficients are given in Tab. 1.

$$v(t) \approx P(t) = \sum_{j=0}^{j=24} a_j t^j \quad (2)$$

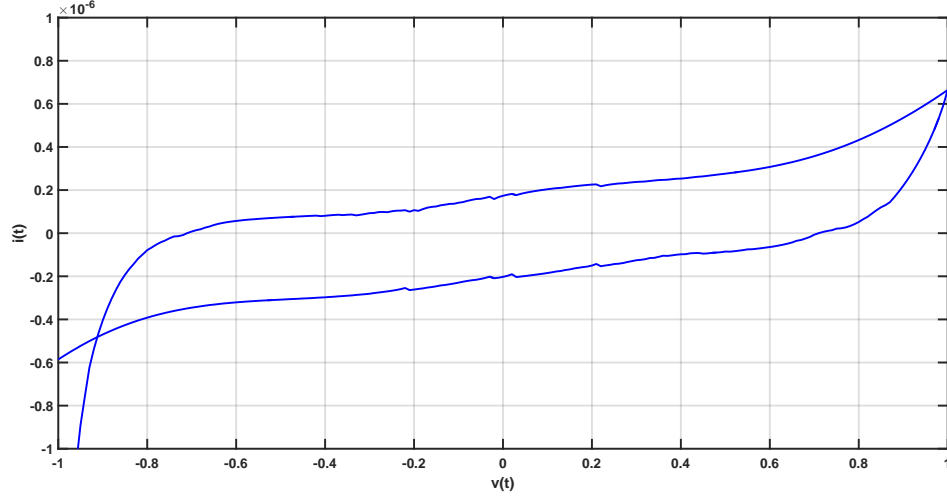


Figure 11: Raw data from average fruit bodies I-V cyclic voltammetry performed over -1 V to 1 V. Stem-to-cap electrode placement.

Table 1: **Coefficient of P(t)**

$a_0$	2.36810109946699e-43	$a_{13}$	1.18302125464207e-12
$a_1$	-4.78342788514078e-40	$a_{14}$	-6.72265349925510e-11
$a_2$	4.45025298649318e-37	$a_{15}$	2.90458838155410e-09
$a_3$	-2.52211206380669e-34	$a_{16}$	-9.51752589043893e-08
$a_4$	9.68672841708898e-32	$a_{17}$	2.33484036114612e-06
$a_5$	-2.64464369703488e-29	$a_{18}$	-4.19159536470121e-05
$a_6$	5.19611819410190e-27	$a_{19}$	0.000531866967507868
$a_7$	-7.12198496974121e-25	$a_{20}$	-0.00453232038841485
$a_8$	5.80230108481181e-23	$a_{21}$	0.0240895989682110
$a_9$	1.59013702626457e-22	$a_{22}$	-0.0726485498614107
$a_{10}$	-8.60157726907686e-19	$a_{23}$	0.135299293073760
$a_{11}$	1.48292987584698e-16	$a_{24}$	-1.04736115240006
$a_{12}$	-1.56317950862153e-14		

Table 2: **Goodness of fit**

Sum of squared estimate of errors	$SSE = \sum_{j=1}^{j=n} (v_j - \hat{v}_j)^2$	0.0680517563652170
Sum of squared residuals	$SSR = \sum_{j=1}^{j=n} (\hat{v}_j - \bar{v})^2$	133.688517134422
Sum of square total	$SST = SSE + SSR$	133.756568890787
Coefficient of determination	$R - \text{square} = \frac{SSR}{SST}$	0.999491226809049

The polynomial fits very well the experimental voltage curve, as the statistical indexes show in Tab, 2. Step 2: in the same way approximate the current  $i(t)$  using a twenty-four-degree polynomial (Fig. 13) whose coefficients are given in Table 3.

$$i(t) \approx Q(t) = \sum_{j=0}^{j=24} b_j t^j \quad (3)$$

Again, the polynomial fits well the experimental intensity curve, as displayed in Table 4. Step 3: From (1) used under the following form  $D_t^{\alpha_2} q(t) \neq 0$ .

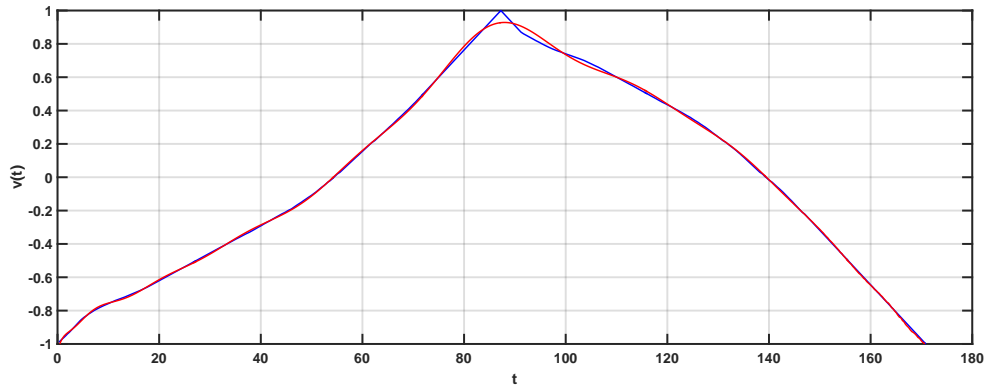


Figure 12: Voltage versus time and its approximation by a 24-degree polynomial

Table 3: Coefficient of  $Q(t)$

$b_0$	8.73846352218898e-49	$b_{13}$	4.25821973203331e-18
$b_1$	-1.71535341852628e-45	$b_{14}$	-2.42471413376463e-16
$b_2$	1.55262364796050e-42	$b_{15}$	1.06306849079070e-14
$b_3$	-8.56384614589988e-40	$b_{16}$	-3.58289124918788e-13
$b_4$	3.19831491989559e-37	$b_{17}$	9.19419585703268e-12
$b_5$	-8.46294727047340e-35	$b_{18}$	-1.76692818009608e-10
$b_6$	1.59708666114599e-32	$b_{19}$	2.48346182702953e-09
$b_7$	-2.04593370725626e-30	$b_{20}$	-2.47326661661364e-08
$b_8$	1.36036443304302e-28	$b_{21}$	1.67584032221916e-07
$b_9$	8.14484000064489e-27	$b_{22}$	-7.34738169887512e-07
$b_{10}$	-3.66183256804588e-24	$b_{23}$	1.95479195837707e-06
$b_{11}$	5.61870303550308e-22	$b_{24}$	-2.69478636561017e-06
$b_{12}$	-5.69947824465678e-20		

Table 4: Goodness of fit

Sum of squared estimate of errors	5.84247524503151e-13
Sum of squared residuals	4.07366051979587e-11
Sum of square total	4.13208527224619e-11
Coefficient of determination	0.985860709883522

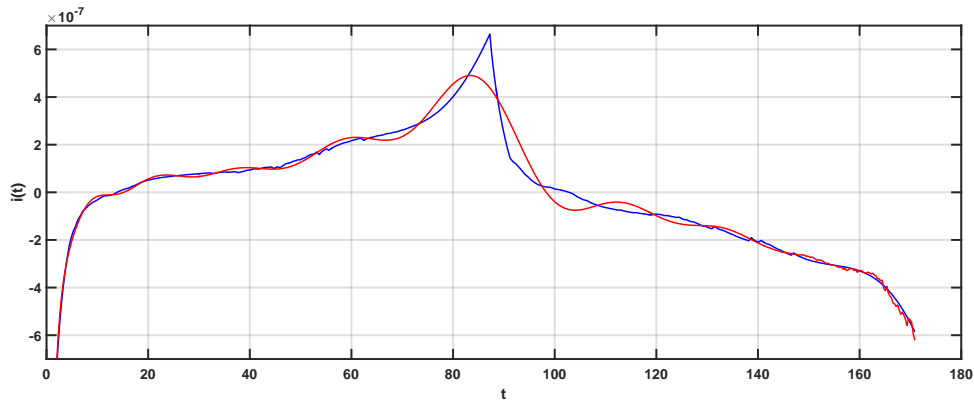


Figure 13: Current versus time and its approximation by a 24 degree polynomial

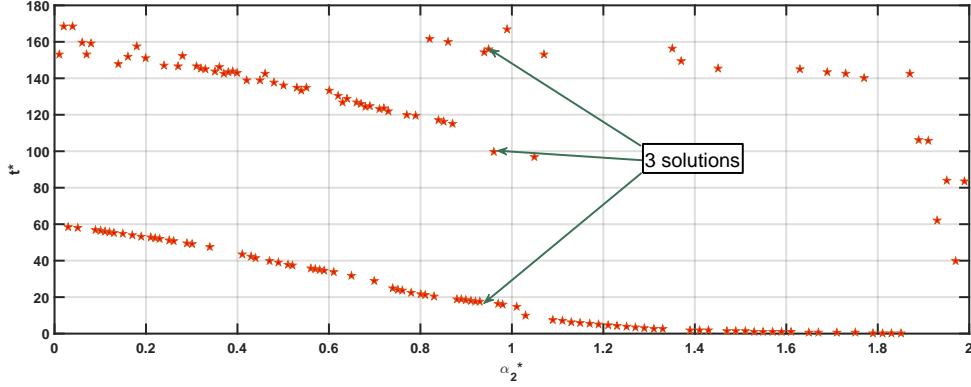


Figure 14: Zeros  $t^*(\alpha_2)$  of the denominator of  $F_M^{\alpha_1, \alpha_2}(t)$ .

$$F_M^{\alpha_1, \alpha_2}(t) = \frac{D_t^{\alpha_1} \varphi t}{D_t^{\alpha_2} q(t)} \quad (4)$$

and the Rieman-Liouville fractional derivative defined by [31]

$${}^{\text{RL}}D_t^\alpha f(t) = \frac{1}{\Gamma(m - \alpha)} \frac{d^m}{dt^m} \int_0^t (t - s)^{m - \alpha - 1} f(s) ds, \quad m - 1 < \alpha < m \quad (5)$$

together with the formula for the power function

$${}^{\text{RL}}D_t^\alpha (at^\beta) = \frac{a\Gamma(\beta + 1)}{\Gamma(\beta - \alpha + 1)} t^{\beta - \alpha}, \quad \beta > -1, \alpha > 0, \quad (6)$$

we obtain the closed formula of  $F_M^{\alpha_1, \alpha_2}(t)$ , approximation of the true biological memfractance of the Oyster mushroom

$$F_M^{\alpha_1, \alpha_2}(t) = \frac{D_t^{\alpha_1} \varphi(t)}{D_t^{\alpha_2} q(t)} = \frac{{}^{\text{RL}}D_t^{\alpha_1} \sum_{j=0}^{j=24} \frac{a_j}{j+1} t^{j+1}}{{}^{\text{RL}}D_t^{\alpha_2} \sum_{j=0}^{j=24} \frac{b_j}{j+1} t^{j+1}} = \frac{\sum_{j=0}^{j=24} \frac{a_j \Gamma(j+1)}{\Gamma(j+2-\alpha_1)} t^{j+1-\alpha_1}}{\sum_{j=0}^{j=24} \frac{b_j \Gamma(j+1)}{\Gamma(j+2-\alpha_2)} t^{j+1-\alpha_2}} \quad (7)$$

Step 4 choice of parameter  $\alpha_1$  and  $\alpha_2$ : We are looking for the best value of these parameters in the range  $(\alpha_1, \alpha_2) \in [0, 2]^2$ . In this goal, we are considering first the singularities of  $F_M^{\alpha_1, \alpha_2}(t)$  in order to avoid their existence, using suitable values of the parameters. Secondly, we will choose the most regular approximation. We compute numerically, the values  $t^*(\alpha_2)$  which vanish the denominator of  $F_M^{\alpha_1, \alpha_2}(t)$  (Fig. 14).

We observe one, two or three coexisting solutions depending on the value of  $\alpha_2$ . Moreover, there is no value of  $\alpha_2$  without zero of the denominator. Therefore, in order to eliminate the singularities, we need to determine the couples  $(\alpha_1, \alpha_2) \in [0, 2]^2$ , vanishing simultaneously denominator and numerator of  $F_M^{\alpha_1, \alpha_2}(t)$  (Figs. 15,16).

In the second part of step 4, we choose the most regular approximation. We consider that the most regular approximation is the one for which the function range ( $F_M^{\alpha_1, \alpha_2}(t)$ ) is minimal (Figs. 17,18)

$$\text{range}(F_M^{\alpha_1, \alpha_2}(t)) = \max_{t \in [0, 171]} (F_M^{\alpha_1, \alpha_2}(t)) - \min_{t \in [0, 171]} (F_M^{\alpha_1, \alpha_2}(t)) \quad (8)$$

From the numerical results, the best couple  $(\alpha_1, \alpha_2)$  and the minimum range of  $F_M^{\alpha_1, \alpha_2}(t)$  are given in Table 5, and the corresponding Memfractance is displayed in Fig. 19.

The value of  $(\alpha_1, \alpha_2)$  given in Table 5 belongs to the triangle of Fig. 10, whose vertices are Memristor, Memcapacitor and Capacitor. Which means that Oyster mushroom fruit bodies with stem to cap electrodes, is like a mix of such basic electronic devices.

As a counter-example of our method for choosing the best possible Memfractance, Fig. 20 displays, the Memfractance for a non-optimal couple  $(\alpha_1, \alpha_2) = (1, 1.78348389322388)$  which presents two singularities.

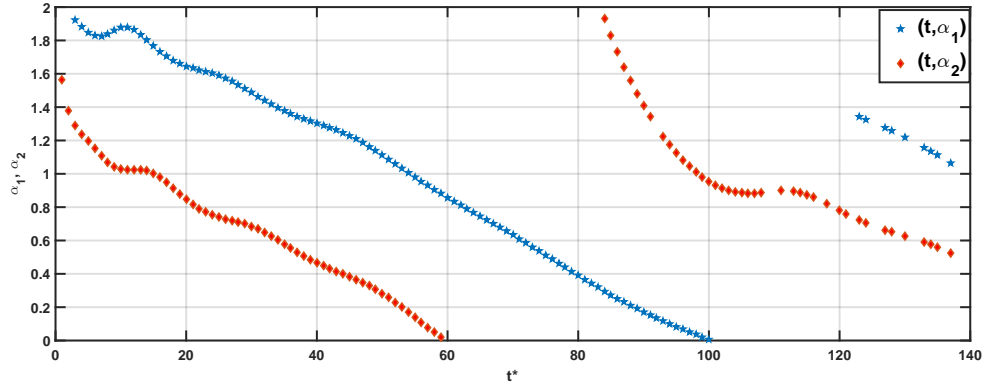


Figure 15: Zeros  $t^*(\alpha_2)$  of  $F_M^{\alpha_1, \alpha_2}(t)$  denominator (red dots), and zeros  $t^*(\alpha_1)$  of the numerator (blue dots).

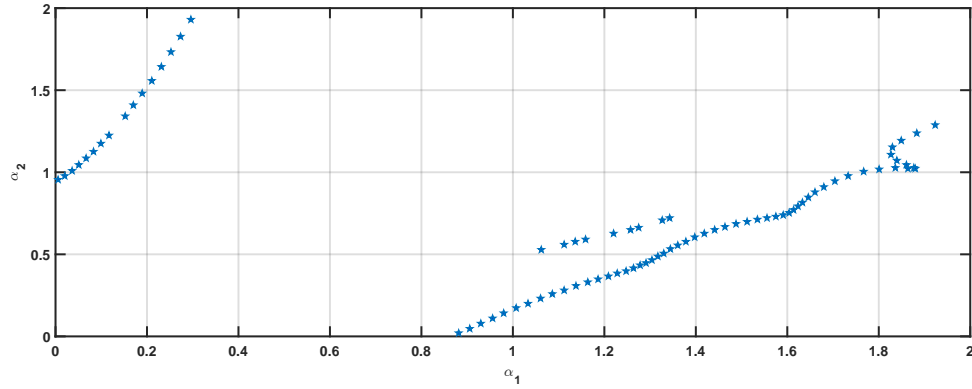


Figure 16: Values of  $(\alpha_1, \alpha_2) \in [0, 2]^2$  for which the zeros  $t^*(\alpha_2)$  of denominator of  $F_M^{\alpha_1, \alpha_2}(t)$  correspond to the zeros  $t^*(\alpha_1)$  of denominator.

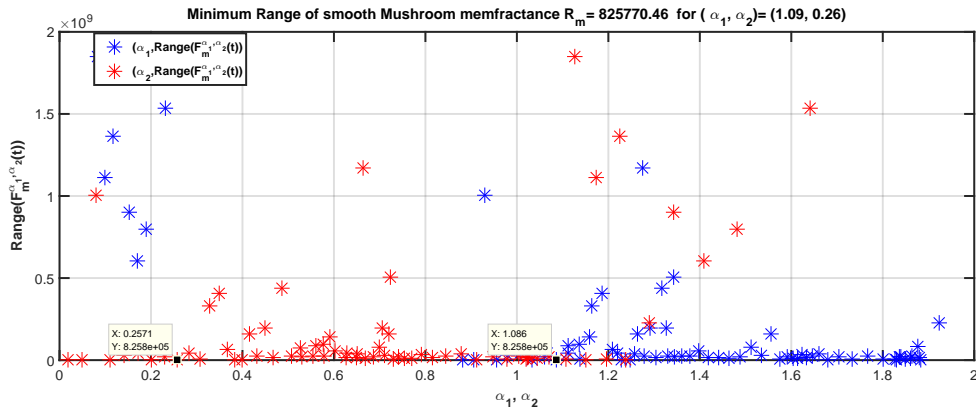


Figure 17: Values of range  $(F_M^{\alpha_1, \alpha_2}(t))$  for  $(\alpha_1, \alpha_2) \in [0, 2]^2$

Table 5: **Minimum**  $F_M^{\alpha_1, \alpha_2}(t)$

$\alpha_1$	$\alpha_2$	Minimum range $F_M^{\alpha_1, \alpha_2}(t)$
1.08642731	0.25709492	825770.46017259

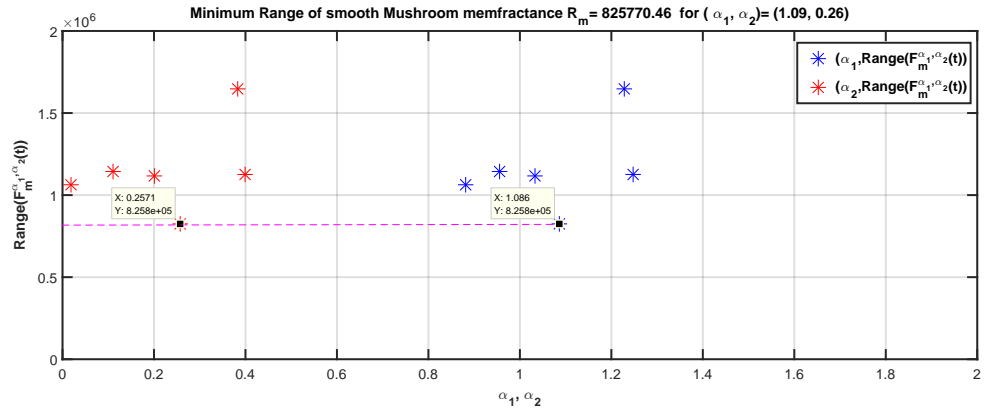


Figure 18: Magnification of Fig. 17.

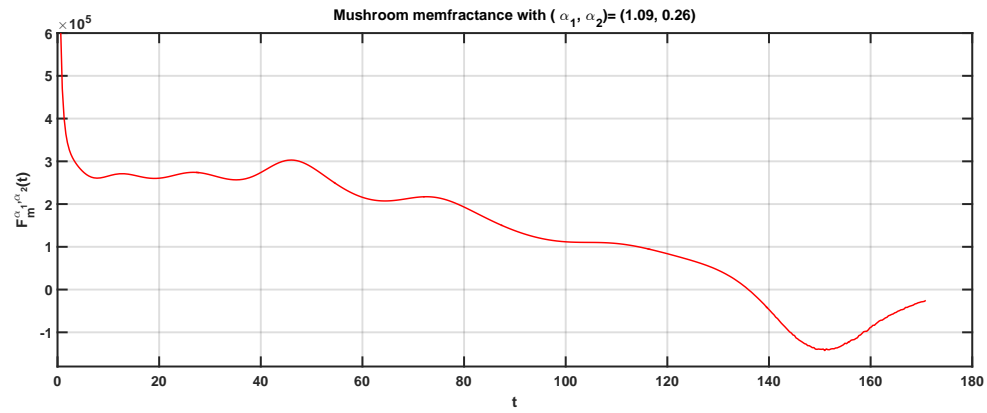


Figure 19: Memfractance for  $(\alpha_1, \alpha_2)$  given in Table 5.

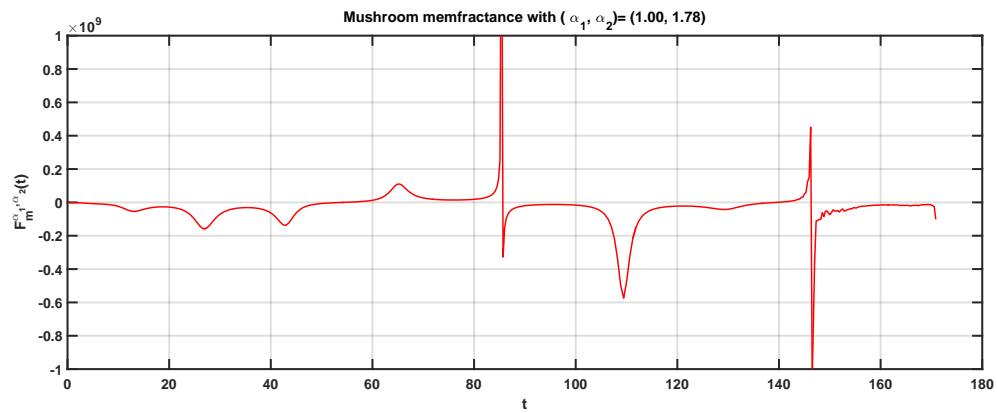


Figure 20: Memfractance with two singularities for  $(\alpha_1, \alpha_2) = (1, 1.78348389322388)$ .

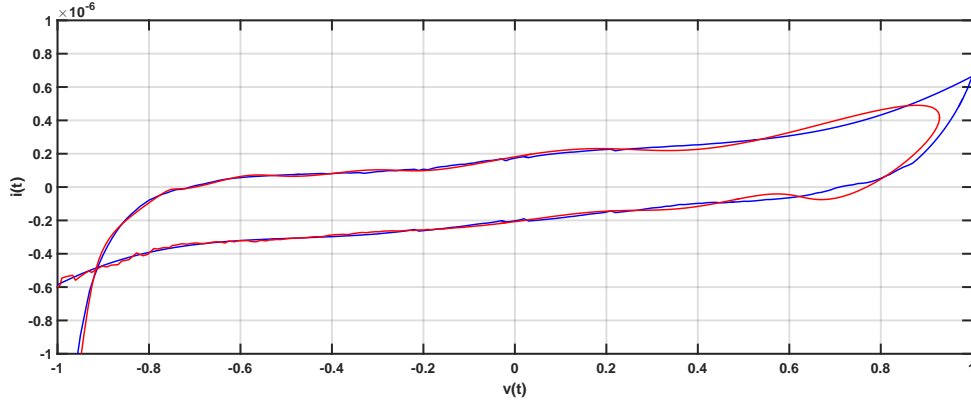


Figure 21: Comparison between average experimental data of cyclic voltammetry performed over -1 V to 1 V, Stem-to-cap electrode placement, and approximate values of  $v(t)$  and  $i(t)$ .

## 4.2 Approximate cycling voltammetry

From the closed formula of  $F_M^{\alpha_1, \alpha_2^*}(t)$  it is possible to retrieve the formula of the current function  $i(t)$  using (1).

$$\begin{aligned}
i(t) &= D_t^{1-\alpha_2} \left[ \frac{D_t^{\alpha_1} \varphi(t)}{F_M^{\alpha_1, \alpha_2}(t)} \right] = D_t^{1-\alpha_2} \left[ \frac{\sum_{j=0}^{j=24} \frac{a_j \Gamma(j+1)}{\Gamma(j+2-\alpha_1)} t^{j+1-\alpha_1}}{\frac{\sum_{j=0}^{j=24} \frac{a_j \Gamma(j+1)}{\Gamma(j+2-\alpha_1)} t^{j+1-\alpha_1}}{\sum_{j=0}^{j=24} \frac{b_j \Gamma(j+1)}{\Gamma(j+2-\alpha_2)} t^{j+1-\alpha_2}}} \right] \\
&= D_t^{1-\alpha_2} \left[ \sum_{j=0}^{j=24} \frac{b_j \Gamma(j+1)}{\Gamma(j+2-\alpha_2)} t^{j+1-\alpha_2} \right] \\
&= \sum_{j=0}^{j=24} \frac{\Gamma(j+2-\alpha_2) b_j \Gamma(j+1)}{\Gamma(j+2-\alpha_2) \Gamma(j+1)} t^{j+1-\alpha_2-(1-\alpha_2)} \\
&= \sum_{j=0}^{j=24} b_j t^j
\end{aligned} \tag{9}$$

The comparison of average experimental data of cyclic voltammetry performed over -1 V to 1 V, Stem-to-cap electrode placement, and closed approximative formula is displayed in Fig. 21, showing a good agreement between both curves except near the maximum value of  $v(t)$  and  $i(t)$ .

Figure 22 shows that the curve computed from closed approximative formula belongs to the histogram of data of all runs.

The discrepancy between both curves is due to the method of approximation chosen in (2) and (3).

It is possible, as we show in the next subsection to improve the fitting of the approximated curve near the right hand-side vertex, using piecewise polynomial approximation of both  $v(t)$  and  $i(t)$ .

## 4.3 Alternative approximation of the cycling voltammetry

Due to the way of conducting the experiments, the voltage curve presents a vertex, that means that the function  $v(t)$  is non-differentiable for  $T = 87.23747459$ . In fact, the value of  $T$  is the average value of the non-differentiable points for the 20 runs.

In this alternative approximation, we follow the same 4 steps as in 4.1, changing the approximation by a twenty-four-degree polynomial to an approximation by a 2-piecewise fifth-degree-polynomial, for both  $v(t)$  and  $i(t)$ .

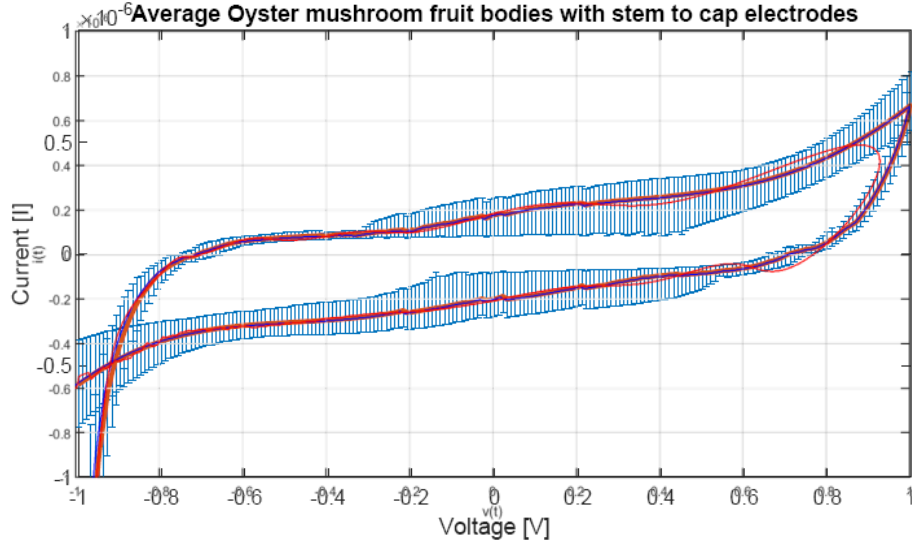


Figure 22: Both average experimental data curve and the curve computed from closed approximative formula are nested into the histogram of data of all runs.

Table 6: **Coefficient for  $i(t)$**

Coefficient	Value for $0 \leq t \leq T$	Coefficient	Value for $T \leq t < T$
$a_0$	-0.98299	$a'_0$	37.16955
$a_1$	0.02665	$a'_1$	-1.2986
$a_2$	-5.91565 E -4	$a'_2$	0.01826
$a_3$	1.12211 E -5	$a'_3$	-1.25146 E -4
$a_4$	-6.28483 E -8	$a'_4$	4.12302 E -7
$a_5$	6.9675 E -11	$a'_5$	-5.25359 E -19

Table 7: **Goodness of fit**

Approximation	$t < T$	$t > T$
Coefficient of determination	0.99983	0.9999

First step: approximation of  $v(t)$  by a 2-piecewise fifth-degree-polynomial (Fig. 23) whose coefficients are given in Table 6.

$$v(t) = \begin{cases} P_1(t) = a_0 + a_1 t + a_2 t^2 + a_3 t^3 + a_4 t^4 + a_5 t^5, & \text{for } 0 \leq t \leq T \\ P_2(t) = a'_0 + a'_1 t + a'_2 t^2 + a'_3 t^3 + a'_4 t^4 + a'_5 t^5, & \text{for } T \leq t < 171 \end{cases} \quad (10)$$

The flux is obtained integrating  $v(t)$  versus time.

$$\varphi(t) = \begin{cases} IP_1(t) = a_0 t + \frac{a_1}{2} t^2 + \frac{a_2}{3} t^3 + \frac{a_3}{4} t^4 + \frac{a_4}{5} t^5 + \frac{a_5}{6} t^6, & \text{for } 0 \leq t \leq T \\ IP_2(t) = a'_0 t + \frac{a'_1}{2} t^2 + \frac{a'_2}{3} t^3 + \frac{a'_3}{4} t^4 + \frac{a'_4}{5} t^5 + \frac{a'_5}{6} t^6, & \text{for } T \leq t < 171 \end{cases} \quad (11)$$

The polynomial fits very well the experimental voltage curve, as the statistical indexes show in Table 7.

Step 2: in the same way, one approximates the current  $i(t)$  using a 2-piecewise fifth degree polynomial (Fig. 24) whose coefficients are given in Table 8.

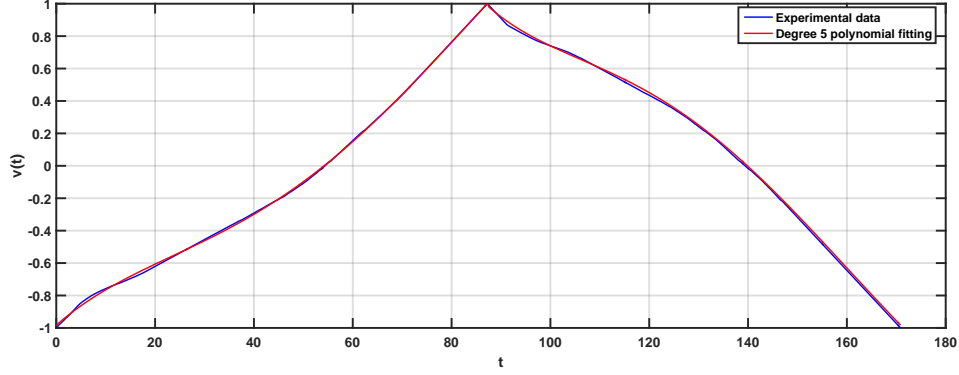


Figure 23: Voltage versus time and its approximation by 2-piecewise fifth degree polynomial

Table 8: **Coefficient for  $i(t)$**

Coefficient	Value for $0 \leq t \leq T$	Coefficient	Value for $T \leq t < 171$
$b_0$	-7.21418 E -7	$b'_0$	2.69466 E -4
$b_1$	1.11765 E -7	$b'_1$	-1.05461 E -5
$b_2$	-6.3792 E -9	$b'_2$	1.63678 E -7
$b_3$	1.57327 E -10	$b'_3$	-1.25915 E -9
$b_4$	-1.7745 E -12	$b'_4$	4.80107 E -12
$b_5$	7.52304 E -15	$b'_5$	-7.26253 E -15

Table 9: **Goodness of fit**

Approximation	$t < T$	$t > T$
Coefficient of determination	0.99171	0.98613

$$i(t) = \begin{cases} P_3(t) = b_0 + b_1 t + b_2 t^2 + b_3 t^3 + b_4 t^4 + b_5 t^5, & \text{for } 0 \leq t \leq T \\ P_4(t) = b'_0 + b'_1 t + b'_2 t^2 + b'_3 t^3 + b'_4 t^4 + b'_5 t^5, & \text{for } T \leq t < 171 \end{cases} \quad (12)$$

Again, the polynomial fits very well the experimental voltage curve, as the statistical indexes show in Table 9.

Therefore, the charge is given by

$$q(t) = \begin{cases} IP_3(t) = b_0 t + \frac{b_1}{2} t^2 + \frac{b_2}{3} t^3 + \frac{b_3}{4} t^4 + \frac{b_4}{5} t^5 + \frac{b_5}{6} t^6, & \text{for } 0 \leq t \leq T \\ IP_4(t) = b'_0 t + \frac{b'_1}{2} t^2 + \frac{b'_2}{3} t^3 + \frac{b'_3}{4} t^4 + \frac{b'_4}{5} t^5 + \frac{b'_5}{6} t^6, & \text{for } T \leq t < 171 \end{cases} \quad (13)$$

Step 3: Following the same calculus as before with (4), one obtains

$$\text{for } 0 \leq t \leq T, F_M^{\alpha_1, \alpha_2}(t) = \frac{{}_0^R L D_t^{\alpha_1} \varphi(t)}{{}_0^R L D_t^{\alpha_2} q(t)} = \frac{{}_0^R L D_t^{\alpha_1} [IP_1(t)]}{{}_0^R L D_t^{\alpha_2} [IP_3(t)]} = \frac{\sum_{j=1}^{j=5} \frac{a_j \Gamma(j+1)}{\Gamma(j+2-\alpha_1)} t^{j+1-\alpha_1}}{\sum_{j=0}^{j=5} \frac{b_j \Gamma(j+1)}{\Gamma(j+2-\alpha_2)} t^{j+1-\alpha_2}} \quad (14)$$

However, because fractional derivative has memory effect, for  $T < t < 171$ , the formula is slightly more complicated

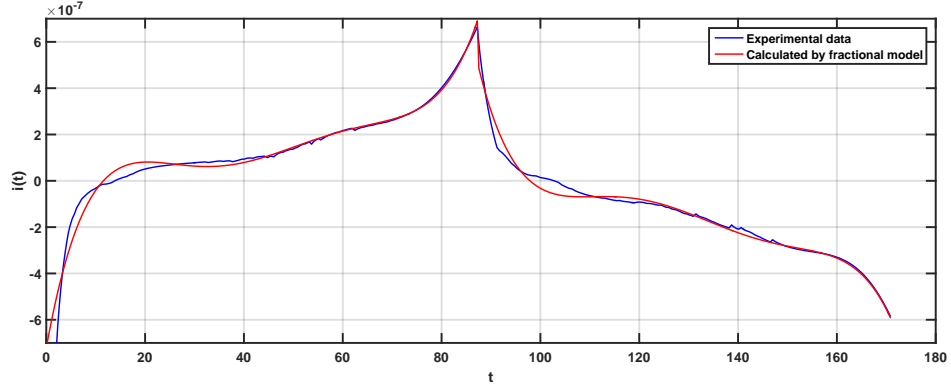


Figure 24: Current versus time and its approximation by 2-piecewise fifth degree polynomial

$$\begin{aligned}
F_M^{\alpha_1, \alpha_2}(t) &= \frac{{}_0^{RL}D_t^{\alpha_1} \varphi(t)}{{}_0^{RL}D_t^{\alpha_2} q(t)} = \frac{\frac{1}{\Gamma(m_1 - \alpha_1)} \frac{d^{m_1}}{dt^{m_1}} \int_0^t (t-s)^{m_1 - \alpha_1 - 1} \varphi(s) ds}{\frac{1}{\Gamma(m_2 - \alpha_2)} \frac{d^{m_2}}{dt^{m_2}} \int_0^t (t-s)^{m_2 - \alpha_2 - 1} q(s) ds}, \quad m_1 - 1 < \alpha_1 < m_1 \text{ and } m_2 - 1 < \alpha_2 < m_2 \\
&= \frac{\frac{1}{\Gamma(m_1 - \alpha_1)} \frac{d^{m_1}}{dt^{m_1}} \left[ \int_0^T (t-s)^{m_1 - \alpha_1 - 1} IP_1(s) ds + \int_T^t (t-s)^{m_1 - \alpha_1 - 1} IP_2(s) ds \right]}{\frac{1}{\Gamma(m_2 - \alpha_2)} \frac{d^{m_2}}{dt^{m_2}} \left[ \int_0^T (t-s)^{m_2 - \alpha_2 - 1} IP_3(s) ds + \int_T^t (t-s)^{m_2 - \alpha_2 - 1} IP_4(s) ds \right]} \\
&= \frac{\frac{1}{\Gamma(m_1 - \alpha_1)} \frac{d^{m_1}}{dt^{m_1}} \sum_{j=0}^{j=5} \left[ \frac{a_j}{j+1} \int_0^T (t-s)^{m_1 - \alpha_1 - 1} s^{j+1} ds + \frac{a'_j}{j+1} \int_T^t (t-s)^{m_1 - \alpha_1 - 1} s^{j+1} ds \right]}{\frac{1}{\Gamma(m_2 - \alpha_2)} \frac{d^{m_2}}{dt^{m_2}} \sum_{j=0}^{j=5} \left[ \frac{b_j}{j+1} \int_0^T (t-s)^{m_2 - \alpha_2 - 1} s^{j+1} ds + \frac{b'_j}{j+1} \int_T^t (t-s)^{m_2 - \alpha_2 - 1} s^{j+1} ds \right]} \quad (15)
\end{aligned}$$

Using integration by part repeatedly six times we obtain



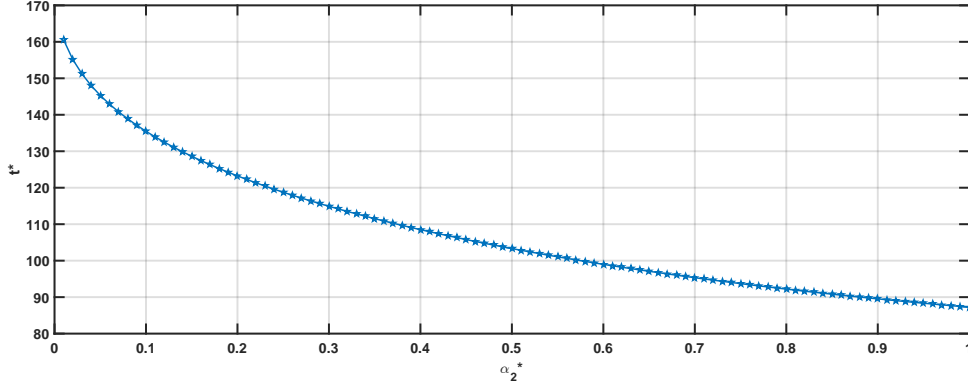


Figure 25: The first zero  $t^*(\alpha_2) \geq T$ , of the denominator of  $F_M^{\alpha_1, \alpha_2}(t)$ , as function of  $\alpha_2$ .

In this 2-piece wise approximation, the vertex is non-differentiable, this implies that (16) expression has a singularity at  $T$  (because  $(t - T)^{-\alpha_1, 2} \rightarrow \infty$ ).

It could be possible to avoid this singularity, using a 3-piece wise approximation, smoothing the vertex. However, the calculus are very tedious. We will explain, below, what our simpler choice implies.

$$\begin{aligned}
 \text{Then } F_M^{\alpha_1, \alpha_2}(t) &= \frac{(t - T)^{-\alpha_1} \left[ \sum_{j=0}^{j=5} \left[ (a'_j - a_j) \sum_{k=0}^{k=j+1} \left[ \frac{j!(t-T)^k T^{j+1-k}}{(j+1-k)! \Gamma(k+1-\alpha_1)} \right] + a_j \frac{j! t^{j+1-\alpha_1} (t-T)^{\alpha_1}}{\Gamma(j+2-\alpha_1)} \right] \right]}{(t - T)^{-\alpha_2} \left[ \sum_{j=0}^{j=5} \left[ (b'_j - b_j) \sum_{k=0}^{k=j+1} \left[ \frac{j!(t-T)^k T^{j+1-k}}{(j+1-k)! \Gamma(k+1-\alpha_2)} \right] + b_j \frac{j! t^{j+1-\alpha_2} (t-T)^{\alpha_2}}{\Gamma(j+2-\alpha_2)} \right] \right]} \\
 &= \frac{\sum_{j=0}^{j=5} \left[ (a'_j - a_j) \sum_{k=0}^{k=j+1} \left[ \frac{j!(t-T)^k T^{j+1-k}}{(j+1-k)! \Gamma(k+1-\alpha_1)} \right] + a_j \frac{j! t^{j+1-\alpha_1} (t-T)^{\alpha_1}}{\Gamma(j+2-\alpha_1)} \right]}{(t - T)^{\alpha_1 - \alpha_2} \sum_{j=0}^{j=5} \left[ (b'_j - b_j) \sum_{k=0}^{k=j+1} \left[ \frac{j!(t-T)^k T^{j+1-k}}{(j+1-k)! \Gamma(k+1-\alpha_2)} \right] + b_j \frac{j! t^{j+1-\alpha_2} (t-T)^{\alpha_2}}{\Gamma(j+2-\alpha_2)} \right]}
 \end{aligned} \tag{17}$$

Finally

$$F_M^{\alpha_1, \alpha_2}(t) = \begin{cases} \frac{\sum_{j=0}^{j=5} \frac{a_j \Gamma(j+1)}{\Gamma(j+2-\alpha_1)} t^{j+1-\alpha_1}}{\sum_{j=0}^{j=5} \frac{b_j \Gamma(j+1)}{\Gamma(j+2-\alpha_2)} t^{j+1-\alpha_2}}, & \text{for } 0 \leq t \leq T \\ \frac{\sum_{j=0}^{j=5} \left[ (a'_j - a_j) \sum_{k=0}^{k=j+1} \left[ \frac{j!(t-T)^k T^{j+1-k}}{(j+1-k)! \Gamma(k+1-\alpha_1)} \right] + a_j \frac{j! t^{j+1-\alpha_1} (t-T)^{\alpha_1}}{\Gamma(j+2-\alpha_1)} \right]}{(t-T)^{\alpha_1 - \alpha_2} \sum_{j=0}^{j=5} \left[ (b'_j - b_j) \sum_{k=0}^{k=j+1} \left[ \frac{j!(t-T)^k T^{j+1-k}}{(j+1-k)! \Gamma(k+1-\alpha_2)} \right] + b_j \frac{j! t^{j+1-\alpha_2} (t-T)^{\alpha_2}}{\Gamma(j+2-\alpha_2)} \right]}, & \text{for } T < t < 171 \end{cases} \tag{18}$$

Step 4 choice of parameter  $\alpha_1$  and  $\alpha_2$ : Following the same idea as for the first alternative, we try to avoid singularity for  $F_M^{\alpha_1, \alpha_2}(t)$ , except of course the singularity near  $T$ , which is of mathematical nature (non-differentiability of voltage and intensity at  $t = T$ ). Figure 25 display the first zero  $t^*(\alpha_2) \geq T$ , of the denominator of  $F_M^{\alpha_1, \alpha_2}(t)$ . One can see that  $t^*(1) \cong T$ .

Figure 26 displays the curves of couples  $(\alpha_1, \alpha_2)$  for which the denominator and numerator of  $F_M^{\alpha_1, \alpha_2}(t)$  are null simultaneously for  $t < T$  and  $t > T$ . On this figure, the value of  $\alpha_1$ , that corresponds to  $\alpha_2 = 1$  is  $\alpha_1 \approx 1.78348389322388$ . The corresponding Memfractance is displayed in Fig. 27.

The singularity observed in Figs. 27-28 is due to the non-differentiability of both voltage and intensity functions at point  $T$ . It is only a mathematical problem of approximation which can be solved using a 3-piecewise polynomial instead of the 2-piecewise polynomial  $(P1(t), P2(t))$  and  $(P3(t), P4(t))$ . The third added piecewise polynomials for  $v(t)$  and  $i(t)$  being defined on the tiny interval [87.24, 87.90]. However due to more tedious calculus, we do not consider this option in the present article. It is only a math problem, and one can consider that Fig. 28 represents the value of the memfractance in the interval  $[0, 87.24] \cup [87.90, 171]$ .

The value of  $(\alpha_1 = 1.78, \alpha_2 = 1.00)$  belongs to the line segment of Fig. 10, whose extremities are Memristor, and Capacitor. Which means that Oyster mushroom fruit bodies with stem to cap electrodes, is like a mix of such basic electronic devices. The comparison of average experimental data of cyclic voltammety

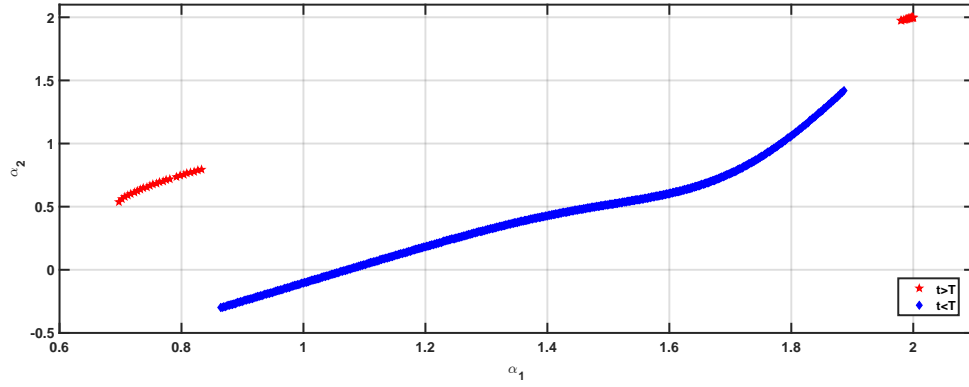


Figure 26: Couples  $(\alpha_1, \alpha_2)$  for which the denominator and numerator of  $F_M^{\alpha_1, \alpha_2}(t)$  are null simultaneously for  $t < T$  (blue dot) and  $t > T$  (red dot).

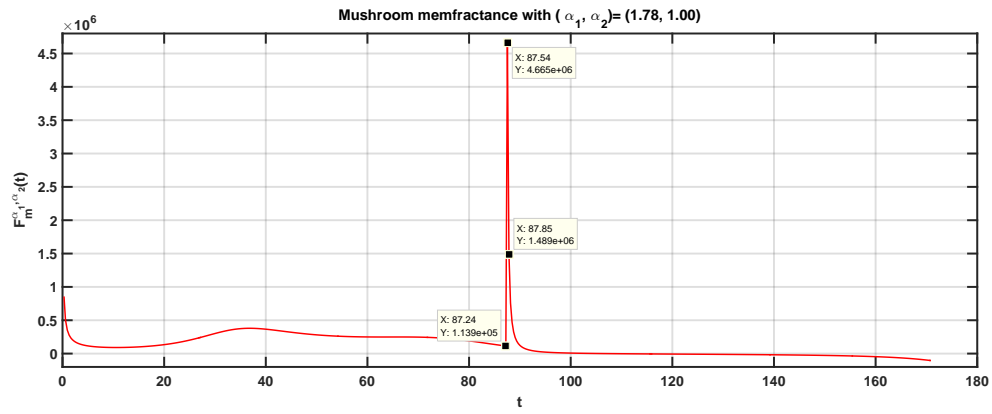


Figure 27: Memfractance for  $(\alpha_1 = 1.78, \alpha_2 = 1.00)$  given in Table 5

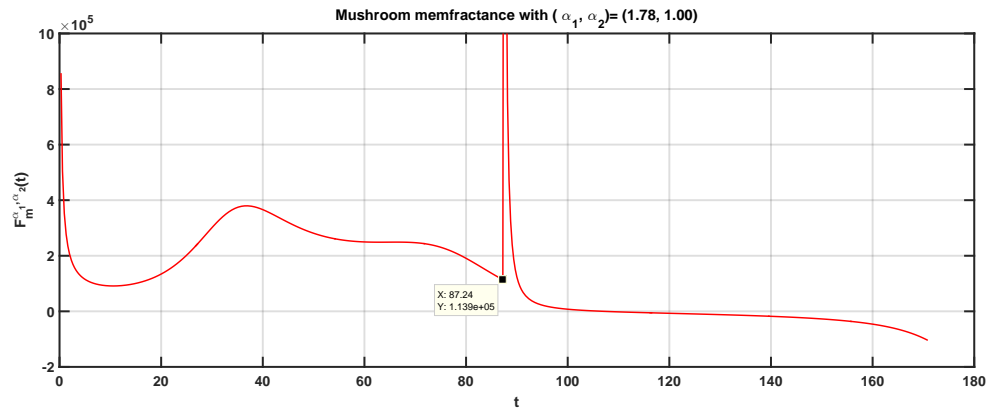


Figure 28: Magnification of Fig. 27

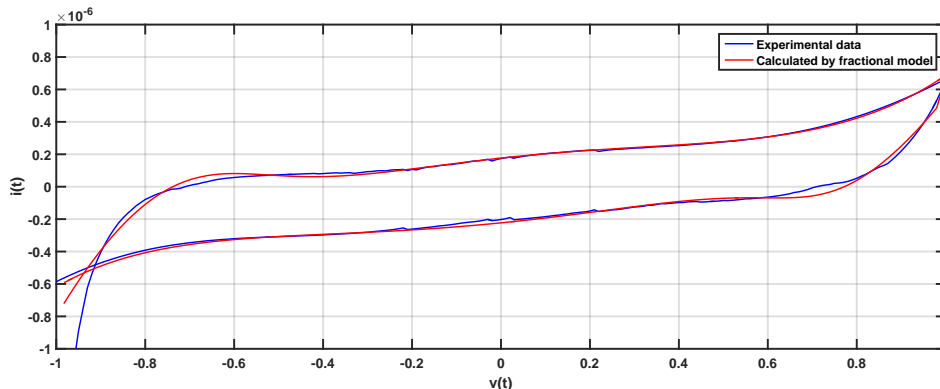


Figure 29: Comparison between average experimental data of cyclic voltammetry performed over -1 V to 1 V, Stem-to-cap electrode placement, and closed approximative formula.

performed over -1 V to 1 V, Stem-to-cap electrode placement, and closed approximative formula is displayed in Fig. 29, showing a very good agreement between both curves.

## 5 Discussion

First at all, we have two remarks:

1. Both approximations used in Section 4 converge to Memfractance with parameter value  $(\alpha_1, \alpha_2)$  - belonging inside or on edge of the triangle of Fig. 10, whose vertices are Memristor, Memcapacitor and Capacitor.

Of course, the value for these approximations are not exactly the same. This is due, in part to the fact that we consider that the most regular approximation is the one for which the function range  $(F_M^{\alpha_1, \alpha_2}(t))$  is minimal. Other choices based on physiology of Mushroom could be invoked. Moreover, the Memfractance is computed on the averaged curve of 20 runs which do not present exactly the same characteristic voltammetry. Oyster mushroom fruit bodies are biological material, which prevent exact reproduction of electrical property.

2. The use of fractional derivatives to analyze the memfractance, is obvious if one considers that fractional derivatives have memory, which allow a perfect modeling of memristive elements. Their handling is however delicate if one wants to avoid any flaw.

Similar I-V characteristics have been experienced for slime mould [15] and apples [36]. The cyclic voltammetry experiments demonstrate that the I-V curve produced from these living substrates is a closed loop where the negative path does not match the positive path. Hence the fungi display the characteristics of a memristor. A similar conclusion is drawn for the microtubule experiments [8]. The microtubule exhibits different resistive properties for the same applied voltage depending on the history of applied voltages.

Additionally, the fruit bodies produce current oscillations during the cyclic voltammetry. This oscillatory effect is only observed on one phase of the voltammetry for a given voltage range which is, again, a behaviour that can be associated to a device whose resistance is a function of its previous resistance. This spiking activity is typical of a device that exhibits memristive behaviours. Firstly, it was reported in experiments with electrochemical devices using graphite reference electrodes, that a temporal dependence of the current of the device - at constant applied voltage - causes charge accumulation and discharge [14]. The spiking is also apparent in some plots, for a large electrode size, in experiments with electrode metal on solution-processed flexible titanium dioxide memristors [17]. A detailed analysis of types of spiking emerging in simulated memristive networks was undertaken in [16]. Repeatable observations of the spiking behaviour in I-V of the fungi is very important because this opens new pathways for the implementation of neuromorphic computing with fungi. A fruitful theoretical foundation of this field is already well developed [34, 21, 32, 30, 27, 22].

## 6 Conclusion

The fruit bodies of grey oyster fungi *Pleurotus ostreatus* were subjected to I-V characterisation a number of times, from which it was clearly shown that they exhibit mem-fractor properties. Under cyclic voltammetry, the fruit body will conduct differently depending on the phase (positive or negative) of the voltammetry. This behaviour produces the classic “lobes” in the I-V characteristics of a memristor.

However, a biological medium, such as the fruit body of the grey oyster fungi presented here, will differ from that of the ideal memristor model since the “pinching” behaviour and size of the hysteresis lobes are functions of the frequency of the voltage sweep as well as the previous resistance. Typically, the biological medium generates its own potential across the electrodes, therefore, even when no additional potential is supplied, there is still current flow between the probes. This property of the fungi produces an opening in the I-V curve that is a classic property of the mem-capacitor. Since the fungi are exhibiting properties of both memristors and mem-capacitors, their electrical memory behaviour puts them somewhere in the mem-fractor solution space where  $0 < \alpha_1, \alpha_2 < 1$ . Hence, it has been shown that fungi act as mem-fractors.

## Acknowledgement

This project has received funding from the European Union’s Horizon 2020 research and innovation programme FET OPEN “Challenging current thinking” under grant agreement No 858132.

## Author contributions

A.A. conceived the idea of experiments. A.A. and A.P. prepared the substrate colonised by mycelium. A.B. performed experiments, collected data and produced all plots in the manuscript. R.L. and MS.A. derived the mathematical model of mem-fractance as seen in grey oyster fungi. All authors prepared manuscript (wrote and reviewed all contents).

## References

- [1] M.-S. Abdelouahab, R. Lozi, and L. Chua. Memfractance: a mathematical paradigm for circuit elements with memory. *International Journal of Bifurcation and Chaos*, 24(9):1430023, 2014.
- [2] Andrew Adamatzky. On spiking behaviour of oyster fungi pleurotus djamor. *Scientific reports*, 8(1):1–7, 2018.
- [3] Andrew Adamatzky. Towards fungal computer. *Interface focus*, 8(6):20180029, 2018.
- [4] Andrew Adamatzky, Phil Ayres, Gianluca Belotti, and Han Wosten. Fungal architecture. *arXiv preprint arXiv:1912.13262*, 2019.
- [5] Nariman A.Khalil, Lobna A.Said, Ahmed G.Radwan, and Ahmed M.Solimane. General fractional order mem-elements mutators. *International Journal of Bifurcation and Chaos*, 90:211–221, 2019.
- [6] Julien Borghetti, Zhiyong Li, Joseph Straznicky, Xuema Li, Douglas AA Ohlberg, Wei Wu, Duncan R Stewart, and R Stanley Williams. A hybrid nanomemristor/transistor logic circuit capable of self-programming. *Proceedings of the National Academy of Sciences*, 106(6):1699–1703, 2009.
- [7] Julien Borghetti, Gregory S Snider, Philip J Kuekes, J Joshua Yang, Duncan R Stewart, and R Stanley Williams. ‘memristive’ switches enable ‘stateful’ logic operations via material implication. *Nature*, 464(7290):873–876, 2010.
- [8] Alessandro Chiolerio, Thomas C. Draper, Richard Mayne, and Andrew Adamatzky. On resistance switching and oscillations in tubulin microtubule droplets. *Journal of Colloid and Interface Science*, 560:589–595, Feb 2020.

- [9] Alessandro Chiolerio, Thomas C Draper, Richard Mayne, and Andrew Adamatzky. On resistance switching and oscillations in tubulin microtubule droplets. *Journal of colloid and interface science*, 560:589–595, 2020.
- [10] L. Chua. Memristor-the missing circuit element. *IEEE Transactions on Circuit Theory*, 18(5):507–519, Sep. 1971.
- [11] Leon Chua. If it’s pinched it’s a memristor. *Semiconductor Science and Technology*, 29(10):104001, 2014.
- [12] María del Rocío Cantero, Paula L Perez, Noelia Scarinci, and Horacio F Cantiello. Two-dimensional brain microtubule structures behave as memristive devices. *Scientific reports*, 9(1):1–10, 2019.
- [13] Victor Erokhin, Tatiana Berzina, and Marco P Fontana. Hybrid electronic device based on polyaniline-polyethyleneoxide junction. *Journal of applied physics*, 97(6):064501, 2005.
- [14] Victor Erokhin and Marco P Fontana. Electrochemically controlled polymeric device: a memristor (and more) found two years ago. *arXiv preprint arXiv:0807.0333*, 2008.
- [15] Ella Gale, Andrew Adamatzky, and Ben de Lacy Costello. Slime mould memristors. *BioNanoScience*, 5(1):1–8, 2015.
- [16] Ella Gale, Ben de Lacy Costello, and Andrew Adamatzky. Emergent spiking in non-ideal memristor networks. *Microelectronics Journal*, 45(11):1401–1415, 2014.
- [17] Ella Gale, David Pearson, Steve Kitson, Andrew Adamatzky, and Ben de Lacy Costello. The effect of changing electrode metal on solution-processed flexible titanium dioxide memristors. *Materials Chemistry and Physics*, 162:20–30, 2015.
- [18] JEAN-MARC GINOUX and BRUNO ROSSETTO. The singing arc: The oldest memristor? In Andrew Adamatzky and Guanrong Chen, editors, *Chaos, CNNs, memristors and beyond*. World Scientific, 2013.
- [19] Yenpo Ho, Garng M Huang, and Peng Li. Nonvolatile memristor memory: device characteristics and design implications. In *Proceedings of the 2009 International Conference on Computer-Aided Design*, pages 485–490, 2009.
- [20] Thang Hoang. Memristor model. <https://www.mathworks.com/matlabcentral/fileexchange/25082-memristor-model>, 2020. MATLAB Central File Exchange. Retrieved January 13, 2020.
- [21] Giacomo Indiveri, Bernabé Linares-Barranco, Robert Legenstein, George Deligeorgis, and Themistoklis Prodromakis. Integration of nanoscale memristor synapses in neuromorphic computing architectures. *Nanotechnology*, 24(38):384010, 2013.
- [22] Giacomo Indiveri and Shih-Chii Liu. Memory and information processing in neuromorphic systems. *Proceedings of the IEEE*, 103(8):1379–1397, 2015.
- [23] DH Jennings. Translocation of solutes in fungi. *Biological Reviews*, 62(3):215–243, 1987.
- [24] Shiv Prasad Kosta, Yogesh P Kosta, Mukta Bhatele, YM Dubey, Avinash Gaur, Shakti Kosta, Jyoti Gupta, Amit Patel, and Bhavin Patel. Human blood liquid memristor. *International Journal of Medical Engineering and Informatics*, 3(1):16–29, 2011.
- [25] Shahar Kvatinsky, Dmitry Belousov, Slavik Liman, Guy Satat, Nimrod Wald, Eby G Friedman, Avinoam Kolodny, and Uri C Weiser. Magic—memristor-aided logic. *IEEE Transactions on Circuits and Systems II: Express Briefs*, 61(11):895–899, 2014.
- [26] Shahar Kvatinsky, Guy Satat, Nimrod Wald, Eby G Friedman, Avinoam Kolodny, and Uri C Weiser. Memristor-based material implication (imply) logic: Design principles and methodologies. *IEEE Transactions on Very Large Scale Integration (VLSI) Systems*, 22(10):2054–2066, 2013.

- [27] Bernabe Linares-Barranco, Teresa Serrano-Gotarredona, Luis A Camuñas-Mesa, Jose A Perez-Carrasco, Carlos Zamarreño-Ramos, and Timothee Masquelier. On spike-timing-dependent-plasticity, memristive devices, and building a self-learning visual cortex. *Frontiers in neuroscience*, 5:26, 2011.
- [28] Eike Linn, R Rosezin, Stefan Tappertzhofen, U Böttger, and Rainer Waser. Beyond von neumann—logic operations in passive crossbar arrays alongside memory operations. *Nanotechnology*, 23(30):305205, 2012.
- [29] Ø G Martinsen, S Grimnes, CA Lütken, and GK Johnsen. Memristance in human skin. *Journal of Physics: Conference Series*, 224(1):012071, 2010.
- [30] Matthew D Pickett, Gilberto Medeiros-Ribeiro, and R Stanley Williams. A scalable neuristor built with mott memristors. *Nature materials*, 12(2):114–117, 2013.
- [31] I. Podlubny. *Fractional Differential Equations*. Academic Press, San Diego, 1999.
- [32] Mirko Prezioso, Y Zhong, D Gavrillov, Farnood Merrih-Bayat, Brian Hoskins, G Adam, K Likharev, and D Strukov. Spiking neuromorphic networks with metal-oxide memristors. In *2016 IEEE International Symposium on Circuits and Systems (ISCAS)*, pages 177–180. IEEE, 2016.
- [33] Karl H Schütte. Translocation in the fungi. *The New Phytologist*, 55(2):164–182, 1956.
- [34] Teresa Serrano-Gotarredona, Themistoklis Prodromakis, and Bernabe Linares-Barranco. A proposal for hybrid memristor-CMOS spiking neuromorphic learning systems. *IEEE cIrcuIts and systEms magazInE*, 13(2):74–88, 2013.
- [35] Dmitri B. Strukov, Gregory S. Snider, Duncan R. Stewart, and R. Stanley Williams. The missing memristor found. *Nature*, 453(7191):80–83, May 2008.
- [36] A G. Volkov and V S. Markin. Electrochemistry of gala apples: Memristors in vivo. *Russian Journal of Electrochemistry*, 53(9):1011–1018, Sept. 2017.
- [37] Alexander G Volkov, Clayton Tucket, Jada Reedus, Maya I Volkova, Vladislav S Markin, and Leon Chua. Memristors in plants. *Plant signaling & behavior*, 9(3):e28152, 2014.
- [38] Z. Yin, H. Tian, G. Chen, and L. O. Chua. What are memristor, memcapacitor, and meminductor? *IEEE Transactions on Circuits and Systems II: Express Briefs*, 62(4):402–406, April 2015.